Materials Research Bulletin 47 (2012) 2638–2645

Contents lists available at SciVerse ScienceDirect

Materials Research Bulletin

journal homepage: www.elsevier.com/locate/matresbu

Template-free hydrothermal derived cobalt oxide nanopowders: Synthesis, characterization, and removal of organic dyes

Mostafa Y. Nassar, Ibrahim S. Ahmed *

Chemistry Department, Faculty of Science, Benha University, Benha 13518, Egypt

ARTICLE INFO

Article history:
Received 31 December 2011
Received in revised form 28 March 2012
Accepted 18 April 2012
Available online 25 April 2012

Keywords:
A. Nanostructures
A. Semiconductors
C. X-ray diffraction
C. Thermogravimetric analysis (TGA)
D. Optical properties

ABSTRACT

Pure spinel cobalt oxide nanoparticles were prepared through hydrothermal approach using different counter ions. First, the pure and uniform cobalt carbonate (with particle size of 21.8–29.8 nm) were prepared in high yield (94%) in an autoclave in absence unfriendly organic surfactants or solvents by adjusting different experimental parameters such as: pH, reaction time, temperature, counter ions, and (Co^{2+}:CO_3^{2-}) molar ratios. Thence, the spinel Co_3O_4 (with mean particle size of 30.5–47.35 nm) was produced by thermal decomposition of cobalt carbonate in air at 500 °C for 3 h. The products were characterized by powder X-ray diffraction (XRD), Fourier transform infrared (FTIR), transmission electron microscope (TEM), scanning electron microscope (SEM), and thermal analysis (TA). Also, the optical characteristics of the as-prepared Co_3O_4 nanoparticles revealed the presence of two band gaps (1.45–1.47, and 1.83–1.93 eV). Additionally, adsorption of methylene blue dye on Co_3O_4 nanoparticles was investigated and the uptake% was found to be >99% in 24 h.

1. Introduction

Recently, research into nanomaterials has increased because optical, electrical, magnetic, and catalytic properties of the matters in this nano-size scale are uniquely different from those of their corresponding bulk counterparts [1,2]. Nanomaterials can be synthesized by either physical or chemical methods. Physical methods include physical vapor deposition (PVD) and spray pyrolysis. However, chemical methods include the sol–gel, microemulsion, hydrothermal and non-aqueous synthesis, and chemical vapor deposition (CVD) [3]. Additionally, morphology controlled synthesis has also attracted an intensive interest and becomes a focus in chemical synthetic field because materials with different morphologies but have the same chemical compositions exhibit substantial differences in their properties [4]. In such, nanomaterials with different morphologies and architectures have been synthesized [5].

Cobalt(II, III) oxide (Co_3O_4) is an important magnetic p-type semiconductor, which belongs to normal spinel structure based on a cubic close packing array of oxide ions [6]. Spinel cobalt oxide nanomaterial can be considered as a main target for many inorganic chemists due to its several technological applications such as semiconductors, anode materials in lithium ion rechargeable batteries, solid state sensors, heterogeneous catalysts, electrochromic sensors, energy storage, and magnetic materials [7–9]. Synthesis of Co_3O_4 nanomaterials can be achieved using several experimental approaches, such as sol–gel methods, heat decomposition processes [10], reflux processes [11], and micellar routes [12]. However, these methods are either time consuming or require expensive instruments. Because of its simplicity, low-cost and multiplicate morphologies of products, hydrothermal synthetic route is an appropriate and efficient approach [13].

Nano-sized cobalt oxides with different morphologies have been successfully produced by a hydrothermal or solvothermal process [14–16]. Among them, a two-step approach is often used to synthesize Co_3O_4 crystals; namely, (i) solid precursors are first prepared, and (ii) the precursors are then thermally converted to Co_3O_4 at elevated temperatures [17]. In particular, cobalt-nitrate-hydroxide, cobalt-nitrate-carbonate-hydroxide, cobalt hydroxyoxide, and cobalt hydroxide have been prepared, and then thermally decomposed to make Co_3O_4 [18–20]. However, the reports on synthesis of $CoCO_3$ hydrothermally, and using it to generate Co_3O_4 nanostructures are limited [17,21]. However, we recently reported on the hydrothermal preparation of square-shaped cobalt carbonate, in presence of a surfactant, using urea as a carbonate source but the yield was not high [22]. Additionally, several nanomaterials such as titanium dioxide [23], Fe_3O_4 [24], and cobalt–nickel mixed oxide [25] have been tried as an adsorbent for color removal from the aquatic medium. Consequently, these have prompted us as to study hydrothermal reaction

* Corresponding author. Tel.: +20 122408034; fax: +20 133222578.
E-mail address: isahmed2010@gmail.com (I.S. Ahmed).

0025-5408/$ – see front matter © 2012 Elsevier Ltd. All rights reserved.
http://dx.doi.org/10.1016/j.materresbull.2012.04.070

of another carbonate source with cobalt cations in presence of different counter ions to be able to generalize the methodology.

Herein, as a continuation to our previous investigations, we report for the first time on the simple synthesis of cobalt oxide nanoparticles in different morphologies via a hydrothermal approach. In this work, cobalt carbonate microspheres were hydrothermally prepared in high yield by the reaction of cobalt salt and ammonium carbonate as a cheap carbonate source, in absence of surfactants. Subsequently, pure phase Co_3O_4 nanoparticles are readily obtained by thermal decomposition of the as-prepared cobalt carbonates in air. Adsorption of methylene blue dye on the as-prepared Co_3O_4 nanoparticles has been briefly studied. The current proposed hydrothermal approach has several advantages over our recent reported one [22], where; it does not require expensive and/or environmental unfriendly organic surfactants, pure cobalt carbonate in high yield with different morphologies and at relatively low temperature (120 °C), and pure spinel Co_3O_4 with different morphologies has been prepared. The intermediate products were investigated by using XRD, FT-IR, TGA, and SEM. The obtained cobalt oxide was characterized by means of XRD, FT-IR, UV–vis spectra, and TEM.

2. Experimental

2.1. Materials and reagents

All reagents were of analytical grade and were purchased and used as received without further purification: cobalt chloride ($CoCl_2{\cdot}6H_2O$; Sigma–Aldrich), cobalt sulfate ($CoSO_4{\cdot}7H_2O$; Sigma–Aldrich), cobalt nitrate ($Co(NO_3)_2{\cdot}4H_2O$; Sigma–Aldrich), ammonium carbonate ($(NH_4)_2CO_3$); Fluka), and methylene blue dye (MB; Fluka).

2.2. Synthesis of cobalt carbonate precursor

In a typical synthesis, 3.22 mmol cobalt salt; 0.76 g of cobalt chloride, 0.90 g of cobalt sulfate, or 0.82 g of cobalt nitrate, was dissolved in distilled water (20 mL). Then, an aqueous solution of ammonium carbonate (0.93 g, 9.66 mmol) in distilled water (60 mL) was added dropwise to the stirring cobalt salt solution. The obtained reaction mixture was stirred for 10 min then transferred into a 100 mL stainless steel autoclave with Teflon liner heated at 120 °C for 0.5 h. After being allowed to cool to room temperature naturally, the obtained pink-colored products of cobalt carbonate ($CoCO_3$) were collected, washed with deionized water, then with ethanol several times via centrifugation–redispersion cycles, and then dried in an oven at 60 °C for 24 h to give pink color cobalt carbonate in 94% yield. Note: the cobalt carbonate samples prepared using cobalt sulfate, cobalt chloride, and cobalt nitrate will be referred to as A, B and C, respectively.

2.3. Preparation of cobalt oxide nanoparticles

The as-prepared cobalt carbonates (A–C) were calcined at 500 °C for 3 h to obtain black crystalline cobalt oxide (Co_3O_4) in an electric furnace with different morphologies and the obtained Co_3O_4 will be referred to as D, E and F samples, respectively.

2.4. Characterization

Powder X-ray diffraction (XRD) of the products was measured using an 18 kW diffractometer (Bruker; model D8 Advance) with monochromated Cu-K_α radiation (λ) 1.54178 Å). Morphologies of the prepared samples were studied by scanning electron microscope (JEOL; model JSM-5410). The TEM images were taken on a transmission electron microscope (JEOL; model 1200 EX) at an accelerating voltage of 80 kV. FT-IR spectra were recorded using FT-IR spectrometer (Bomem; model MB157S) from 4000 to 400 cm^{-1} at room temperature. The thermal studies were performed with a thermal analyzer instrument (Shimadzu; model TA-60WS) with a heating rate of 15 °C/min in nitrogen gas. The optical properties were performed using a Jasco UV-vis spectrophotometer (Jasco; model v530).

3. Results and discussion

3.1. Synthesis of cobalt carbonate

3.1.1. X-ray diffraction studies

The hydrothermal reaction of aqueous solution of ammonium carbonate and aqueous solution of cobalt salt with different counter ions such as sulfate, chloride, and nitrate, separately, was studied. Fig. 1(a–c) shows the powder XRD patterns of the as-prepared cobalt carbonate products. The diffraction patterns are corresponding to samples A, B and C, respectively, with optimum reaction conditions: $[Co^{2+}]/[CO_3^{2-}]$ molar ratio of 1:3, temperature of 120 °C, and reaction time of 0.5 h; for each counter ion. The diffraction peaks for each sample can be indexed to the standard patterns of pure cobalt carbonate (space group R3c, JCPDS card 78-0209) [17]. Other peaks for impurities were not detected. The average size of the nanocrystallite was estimated using the Debye–Scherrer formula [26].

$$D = \frac{0.9\lambda}{\beta \cos\theta_B}$$

where, λ, β, and θ_B are the X-ray wavelength, the full width at half maximum (FWHM) of the diffraction peak and the Bragg diffraction angle, respectively. The average particle size increases from 21.8 to 29.8 nm on changing the counter ion from sulfate to nitrate (Fig. S1). Sulfate counter ions gave the lowest particle size

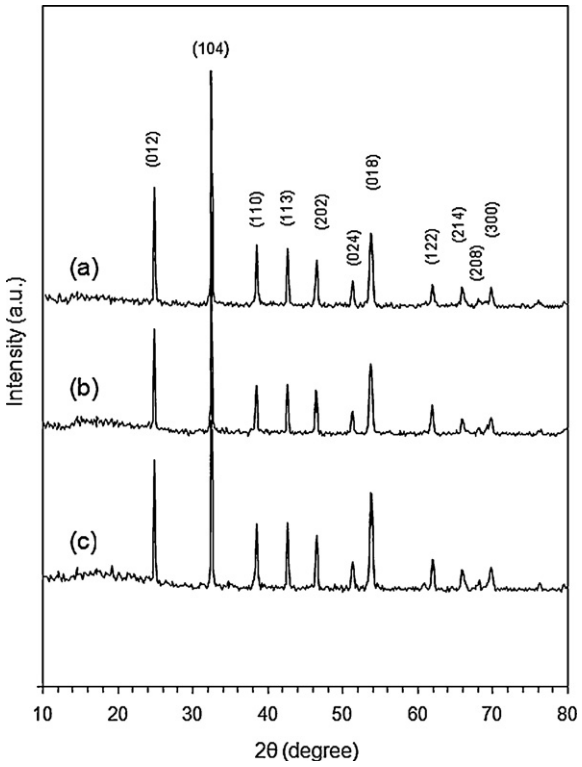

Fig. 1. (a–c) XRD patterns of the $CoCO_3$ products obtained by hydrothermal treatment under the optimal conditions using (a) sulfate, (b) chloride, and (c) nitrate counter ions.

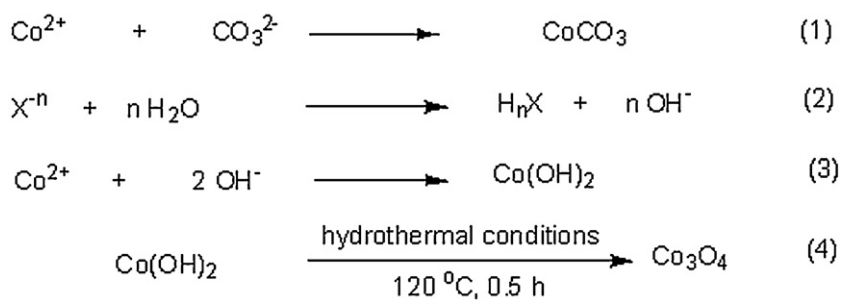

Scheme 1. Proposed mechanism for the formation of cobalt carbonate or a mixture of cobalt carbonate and cobalt oxide; X = sulfate, chloride, or nitrate anion.

because of the lowest particle growth rate of cobalt carbonate precipitation. This can be attributed to the fact that SO_4^{2-} ions are more negatively charged and bulky ions than the other counter ions and, in turn, this can hinder the rate of the particle growth due to the high electrostatic repulsion arising between sulfates and approaching carbonate ions. Additionally, reaction of cobalt cations with carbonate anions in presence of sulfate counter ions may be relatively faster in its beginning which results in an increase in the rate of nucleation. On the other hand, the obtained average particle size in presence of chloride or nitrate counter ions is close, and this may be attributed to the equality of negative charge of the two anions which may be the most predominant factor in this case.

3.1.2. Effect of reaction conditions

Different experimental factors that can affect the synthesis of cobalt carbonate such as $[Co^{2+}]/[CO_3^{2-}]$ molar ratios, reaction temperature and reaction time have been investigated in presence of sulfate, chloride, or nitrate as counter ions, individually. In this investigation, our study focused on the identity of the products and this was followed up using XRD patterns of the products. The counter ion does not have any influence on the identity of the obtained products, and the counter ions under study gave the same results, so that we will present the data obtained for sulfate counter ion only as a representative example.

The $[Co^{2+}]/[CO_3^{2-}]$ molar ratio factor was investigated by carrying out hydrothermal reactions of cobalt sulfate and ammonium carbonate at 160 °C for 24 h, with $[Co^{2+}]/[CO_3^{2-}]$ molar ratios: 1:6, 1:3, 1:1.5, 1:1, and 1:0.5. The XRD patterns (Fig S2) show that the obtained products are pure cobalt carbonate when $[Co^{2+}]/[CO_3^{2-}]$ molar ratio is higher than 1:3 because all the diffraction peaks (Fig. S2(a and b)) can be readily indexed to a pure hexagonal phase of $CoCO_3$ with cell constants: a = 4.661 Å, and c = 14.96 Å, which match well with the standard patterns of cobalt carbonate (space group R3c, JCPDS card 78-0209) [17]. No other peaks for impurities were detected. On the other hand, when molar ratios were lower than 1:3, a mixture of cobalt carbonate and cobalt oxide was formed (Fig. S2(c–e)). Consequently, these results can be explained on the basis of the following proposed mechanism. Hydrolysis of cobalt salt produces OH^- ions according to Eq. (2) (Scheme 1), which provides an alkaline medium for the formation of cobalt hydroxide. At lower molar ratios $\leq$ 1:3 (i.e. lower carbonate concentrations), there is a competition between reactions (1) and (2). Therefore, this competition results in formation of cobalt carbonate and cobalt hydroxide mixture. Then, under the reported hydrothermal conditions, cobalt hydroxide can be converted into cobalt oxide as presented in Eq. (4) (Scheme 1) but cobalt carbonate remains unchanged at the applied temperature, and this produces a mixture of cobalt carbonate and cobalt oxide as reaction products. On the other hand, as the concentration of carbonate ions increases, reaction (1) becomes the more predominant reaction and in turn the amount of cobalt carbonate increases. Moreover, when molar ratio is $\geq$1:3, a pure cobalt carbonate is the only obtained product because the reaction in this case proceeds only according to Eq. (1).

Additionally, to study the effect of reaction time on the hydrothermal synthesis of cobalt carbonate, the hydrothermal reaction of cobalt salt and ammonium carbonate with a molar ratio of 1:3 and at 160 °C was investigated for different reaction times: 24, 18, 12, 6, 3, 1, and 0.5 h. X-ray diffraction patterns (Fig. S3(a–g)) revealed that the products are pure $CoCO_3$ (space group R3c, JCPDS card 78-0209) [17] without impurity phases. By using the Scherrer equation [26], the average particle size of the as-prepared cobalt carbonate samples obtained was estimated, and it was found that the particles size of the as-prepared cobalt carbonate increased from 80 nm to 90 nm, on increasing the reaction time from 0.5 h to 24 h, respectively.

Finally, hydrothermal reaction of interest was studied at 160, 140, 120, 100, and 80 °C (with molar ratio of 1:3 and reaction time of 0.5 h) and the obtained products were characterized using XRD (Fig. S4(a–e)). Upon examination of the XRD patterns, one can notice that the product prepared at 80 °C is not pure cobalt carbonate and has poor crystallinity. After that, on increasing the temperature to 120 °C, the degree of crystallinity increases, and pure cobalt carbonate is produced at 120 °C. Moreover, in the reaction temperature range 120–160 °C, the product is pure cobalt carbonate with good crystallinity, and this temperature range does not have a noticeable effect on the degree of crystallinity. Hence, this investigation can lead us to conclude that 1:3 ($[Co^{2+}]/[CO_3^{2-}]$), 120 °C (reaction temperature), and 0.5 h (reaction time) are the optimal conditions required to hydrothermally prepare a pure cobalt carbonate product.

3.1.3. Morphologies of cobalt carbonate

Morphologies of the prepared cobalt carbonates (A, B, and C samples) under the optimal reaction conditions were investigated using the SEM images as presented in Fig. 2(a–c), respectively. The SEM images show that the three prepared carbonate samples are microspheres whose average diameters are: ca. 4.6, 4.4, and 4.4 μm for A, B, and C, respectively. The enlarged SEM images (Fig. S5(a–c)) revealed that the cobalt carbonate microspheres in the three samples are assembled by small nanocubes with an average sizes: ca. 125, 150, and 150 nm for A, B and C, respectively.

3.1.4. FT-IR spectra

The IR spectra of the as-prepared cobalt carbonate samples are presented in Fig. 3(a–c), for A, B, and C products, respectively. The IR spectra show absorptions at 3326, 3307, and 3242 cm^{-1} for the A, B and C as carbonate products, respectively, which can be assigned to the stretching vibrations of the O–H group of surface molecular water interacting with carbonate anions of the $CoCO_3$ products and the broadness of these bands can be attributed to hydrogen-bonding O–H [27]. The evidence for the presence of CO_3^{2-} in the cobalt carbonate samples is confirmed by its

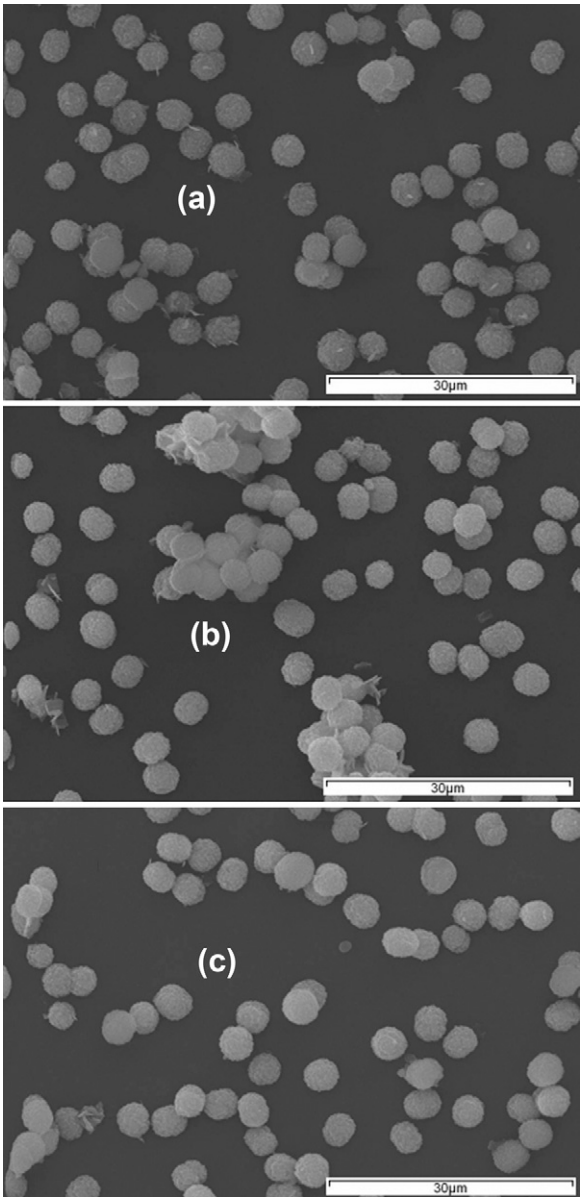

Fig. 2. (a–c) SEM images (low magnification) of the as-prepared $CoCO_3$ by hydrothermal treatment using sulfate counter ions at $[Co^{2+}]/[CO_3^{2-}]$ = 1:3, 120 °C, and for 0.5 h; (a) A-$CoCO_3$, (b) B-$CoCO_3$, and (c) C-$CoCO_3$.

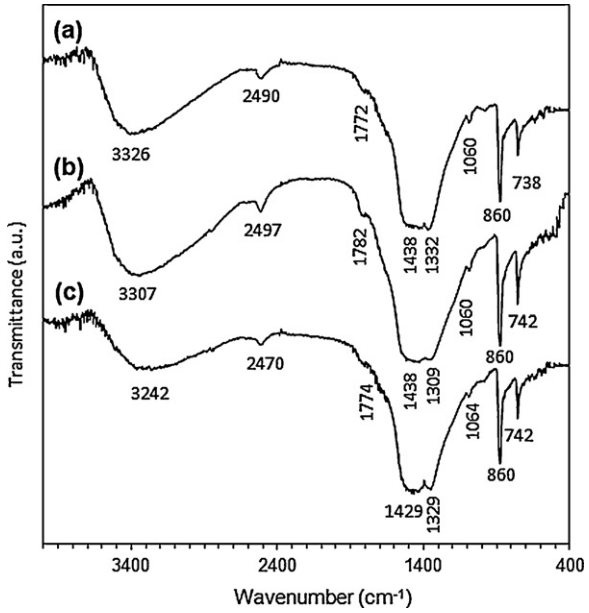

Fig. 3. (a–c) FTIR spectrum of the as-prepared $CoCO_3$; A, B, and C samples.

fingerprint peaks of D_{3h} symmetry at (1438 and 1332), 1060, 860, and 738 cm^{-1} for A sample; at (1438 and 1309), 1060, 860, and 742 cm^{-1} for B sample; and at (1429, and 1329), 1064, 860, and 742 cm^{-1} for C sample; which can be assigned (for each carbonate product) to the vibrational modes of $\nu_3(E)$, $\nu_1(A_1)$, $\nu_2(A_1)$ and $\nu_4(E)$, respectively, according to normal modes of vibration of planar XO_3 molecules/ions (X = C in the present case) [21,28,29]. The band that shown at 2490, 2497 and 2470 cm^{-1} for A, B and C samples, respectively, can also be attributed to vibrational mode of the carbonate anions [30]. Moreover, the shoulder that appeared at 1772, 1782, and 1774 cm^{-1} for A, B and C samples, respectively, can be assigned to an overtone or combination of some vibrational modes of divalent metal ions and the carbonate groups bond [30].

3.1.5. TG–DTA analysis

The thermal behavior of the $CoCO_3$ samples prepared under the optimal conditions has also been investigated by TG–DTA techniques, as presented in Fig. 4(a–c). The TGA curves show that the thermal decomposition behavior of the carbonate samples is similar and each carbonate sample is decomposed in three steps. The first step is attributed to elimination of adsorbed/trapped water and the weight loss for this step is found to be 5.435, 4.264, and 3.722% for A, B and C, respectively. The second step (within the temperature range 140–269, 140–282, and 140–300 °C) corresponds to the loss of 2 mol of CO_2 with mass loss of 22.392, 20.446, and 21.381% for A, B and C samples, respectively, and these values are close to the calculated value (24.6%). The third step takes place within the temperature range 269–500, 282–500, and 300–500 °C which can be attributed to loss of 1 mol of CO with matching mass loss of 8.692, 9.183, and 8.630% (calcd. 7.8%) for A, B and C, respectively. Consequently, the residue of the last mass loss is Co_3O_4. It is worthy to report that the total mass loss of $CoCO_3$ to Co_3O_4 is about 31.084, 29.629 and 30.011%, for A, B and C, respectively, which are close to the calculated value (32.5%). Thermal decomposition of $CoCO_3$ is summarized in Scheme 2. The DTA curves confirmed the results of the TGA curves because the DTA curves exhibited three endothermic peaks at (62.83, 253.2 and 299.3 °C), (56.82, 249.8 and 310.17 °C), and (62.99, 257.99 and 323.56 °C) for A, B and C samples, respectively. The first peak, for each DTA curve, corresponds to elimination of adsorbed/trapped water from the cobalt carbonate sample, the second peak is attributed to loss of CO_2, and the third peak corresponds to loss of carbon monoxide leaving finally Co_3O_4 as a residue.

3.2. Cobalt oxide nanoparticles

3.2.1. Preparation, morphology and spectral characterization

On the basis of the thermal analysis results, the temperature for the thermal conversion of $CoCO_3$ microspheres into Co_3O_4 nanoparticles particles was set at 500 °C for 3 h to ensure the complete decomposition of the $CoCO_3$ precursor. The crystallographic phase of the produced spinel cobalt oxide was confirmed by the XRD method. Upon examination of the XRD pattern as shown in Fig. 5(a–c), all the diffraction peaks can be perfectly assigned to a pure cubic phase of Co_3O_4 products (space group *Fd3m*, lattice constant *a* = 8.084 Å, JCPDS card 74-1657). No peaks for impurities were discerned, indicating the high purity of the produced spinel Co_3O_4. By using the Scherrer equation [26], the

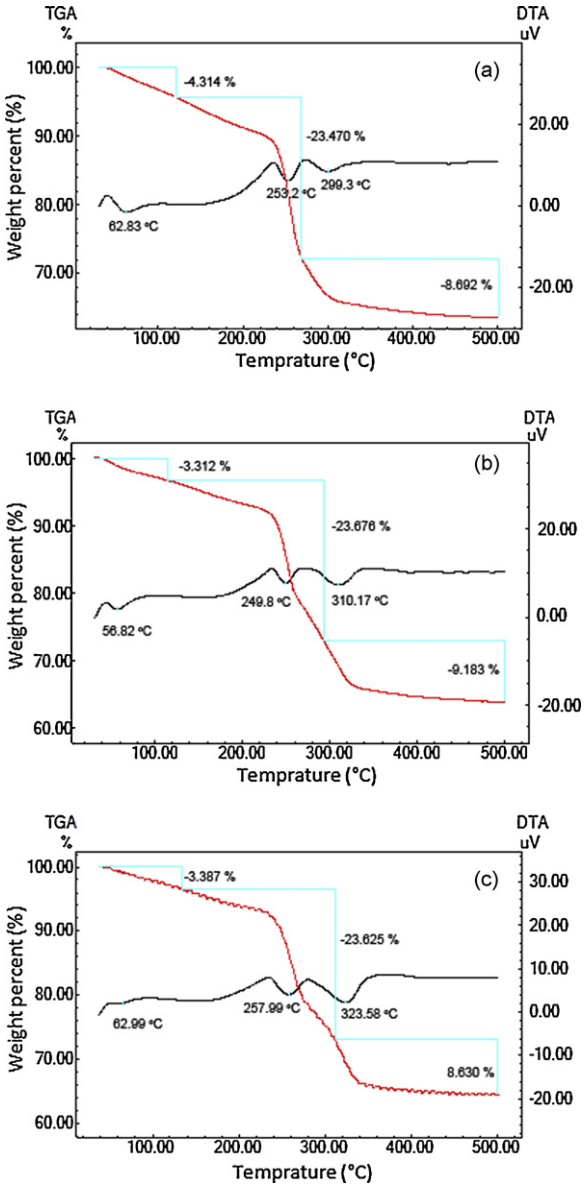

Fig. 4. (a–c) Thermal analyses of the as prepared cobalt carbonate (A, B, and C) samples in nitrogen atmosphere.

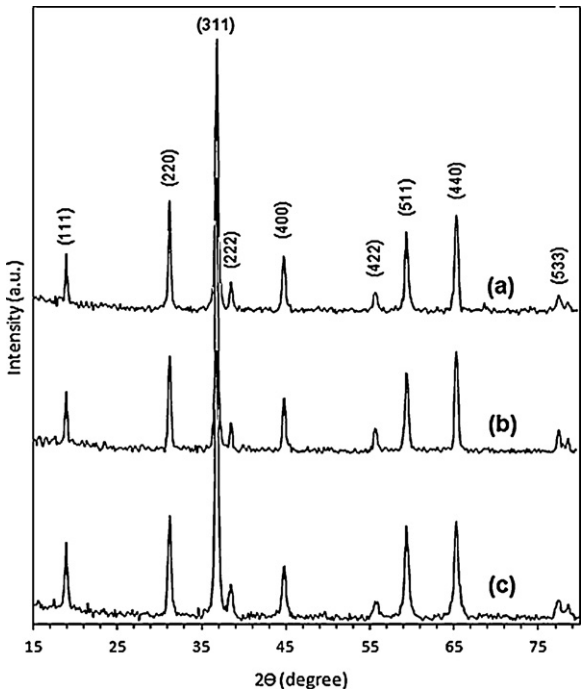

Fig. 5. (a–c) XRD pattern of the obtained Co_3O_4 nanoparticles (D–F) after calcinations at 500 °C in air.

average size of Co_3O_4 nanoparticles was estimated to be ca. 42.3, 47.35, and 30.5 nm for D, E and F samples, respectively.

Morphologies of Co_3O_4 particles were investigated by TEM as presented in Fig. 6(a–c). From the micrograph, it is observed that D–Co_3O_4 particles have almost sheet shapes with diameter range 46–150 nm for oxide D. On the other hand, cobalt oxide E and F have almost hexagon and square shapes with an average diameter of ca.45, and 29 nm for E and F samples, respectively, which is close to the value obtained from the XRD analysis especially the last produced two cobalt oxide products, separately.

The FT-IR spectra of the produced cobalt oxides are presented in Fig. 7(a–c). The IR spectra of the produced cobalt oxide show two strong absorption bands at the same vibration frequencies (659 and 559 cm^{-1}) for D–F oxides which confirm the spinel structure of the produced cobalt oxide, and this also confirms the purity of the as-prepared Co_3O_4 nanoparticles. Specifically, the band appeared at 659 cm^{-1} can be assigned to the stretching vibration mode of M–O bond in which M, Co^{2+}, is tetrahedrally coordinated, while the band appeared at 559 cm^{-1} can be attributed to the M–O bond in which M is Co^{3+} and is octahedrally coordinated [31,32].

3.2.2. Optical properties of cobalt oxide nanoparticles

The optical absorbance properties of the produced cobalt oxide particles were investigated by recording UV–vis absorption spectra (Fig. S6(a–c)) at room temperature. The optical band gap (E_g) of the spinel Co_3O_4 can be calculated using the equation the following equation [33,34]:

$$(\alpha h\nu) = K(h\nu - E_g)^n$$

where α is the absorption coefficient, $h\nu$ is the photon energy, K is a constant involving properties of the bands, E_g is the band gap, and n depends on the kind of optical transitions. Specifically, n is 1/2, 3/2, 2, and 3 for transitions which are directly allowed, directly forbidden, indirectly allowed, and indirectly forbidden, respectively [35]. In this case, $(\alpha h\nu)^2$ is plotted versus $h\nu$ values as shown in Fig. 8(a–c). For each curve, a satisfactory fit was obtained for $(\alpha h\nu)^2$ as a function of $h\nu$, showing the existence of a direct gap.

$$3\,CoCO_3 \xrightarrow[\text{for a, b, c curves, repectively}]{\text{140 - 269, 282, 300 °C}} Co_3(O_2)CO_3 + 2\,CO_2$$

$$Co_3(O_2)CO_3 \xrightarrow[\text{for a, b, c curves, repectively}]{\text{269, 282, 300 - 500 °C}} Co_3O_4 + CO$$

Scheme 2. Proposed thermal degradation mechanism of the as-prepared cobalt carbonate samples in nitrogen atmosphere.

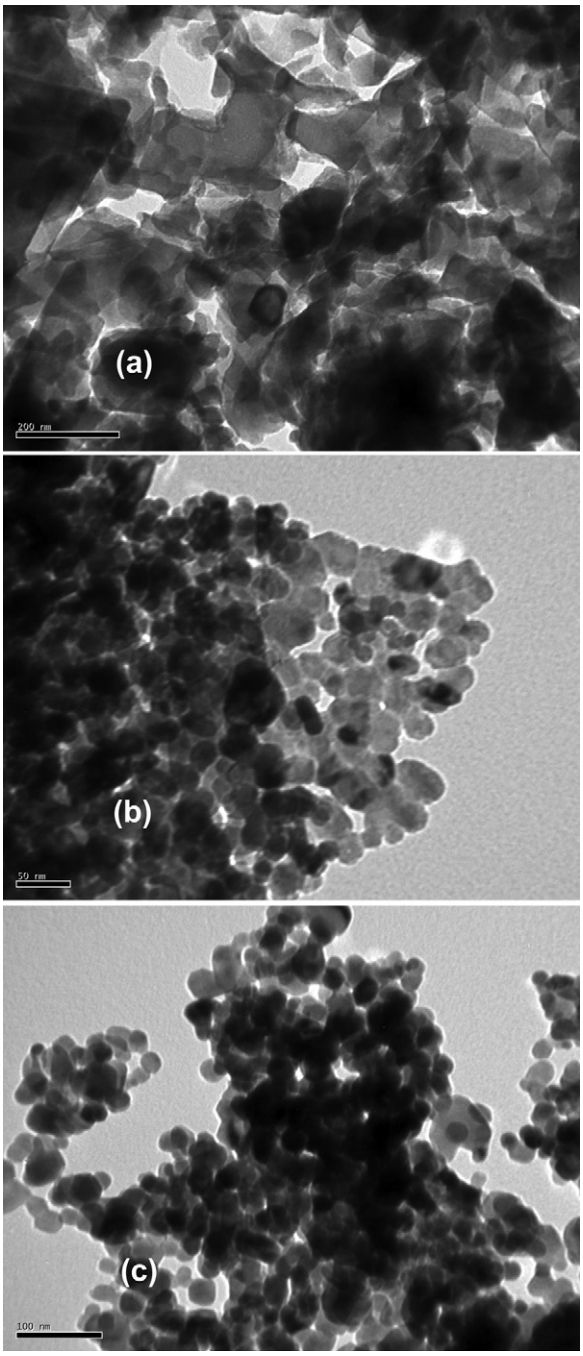

Fig. 6. (a–c) TEM images of the obtained Co_3O_4; D–F, using (a) sulfate, (b) chloride, and (c) nitrate counter ions, respectively.

The extrapolation of each graph to $(\alpha h\nu)^2 = 0$ yields the optical band gap (E_g). The curves presented in Fig. 8(a–c) can be linearly fitted into 2 lines with the intercepts at: (1.85 and 1.45 eV), (1.93 and 1.46 eV), and (1.47 and 1.83 eV) for D, E and F samples, respectively. The optical band gap of 1.85, 1.93, and 1.83 eV for D, E and F samples, respectively, can be assigned to a $O^{2-} \rightarrow Co^{2+}$ charge transfer process (basic optical band gap energy, or valence to conduction band excitation), while the optical band gaps of 1.45, 1.46, and 1.47 eV for D, E and F samples, respectively, can be assigned to $O^{2-} \rightarrow Co^{3+}$ charge transfer (the Co^{3+} level located below the conduction band). The best fit of the previous equation gives $n = 1/2$, suggesting that the obtained Co_3O_4 nanoparticles are semiconducting with a direct transition and these data are in correspondence with the reported ones [22,32–34].

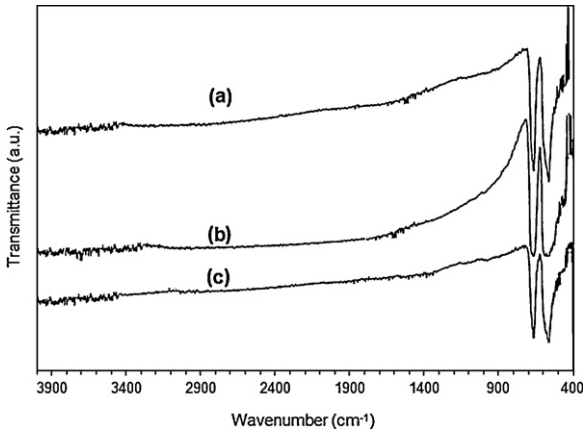

Fig. 7. (a–c) FTIR spectrum of the obtained Co_3O_4 nanoparticles (D–F) after calcinations at 500 °C in air for 3 h.

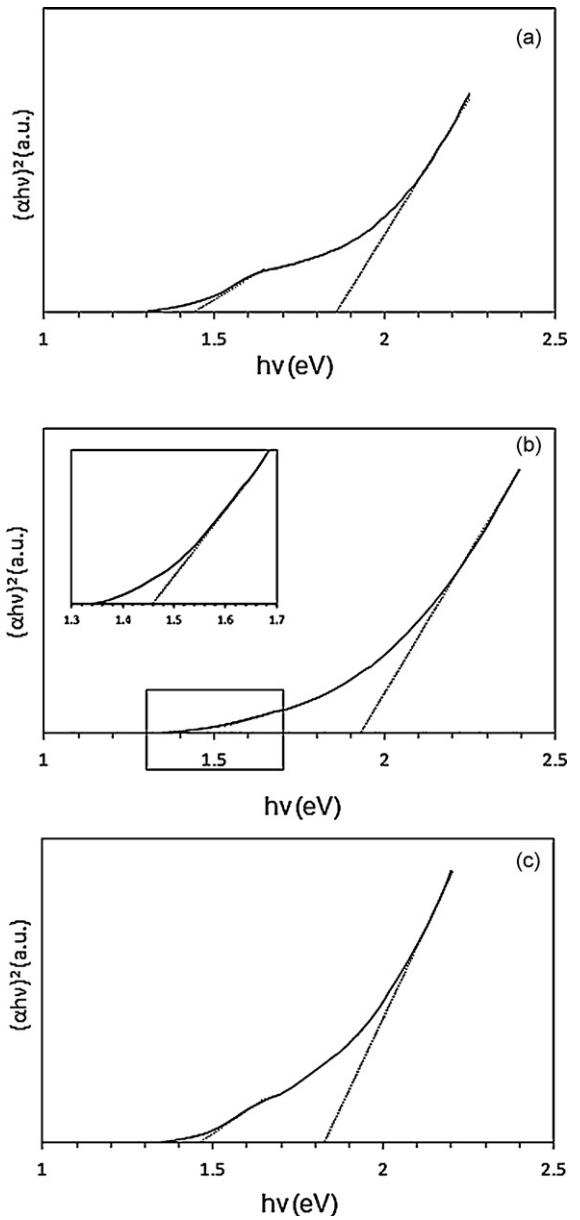

Fig. 8. (a–c) $(\alpha h\nu)^2 \sim h\nu$ curves (a, b, and c) for the prepared cobalt oxide samples (D, E, and F); respectively.

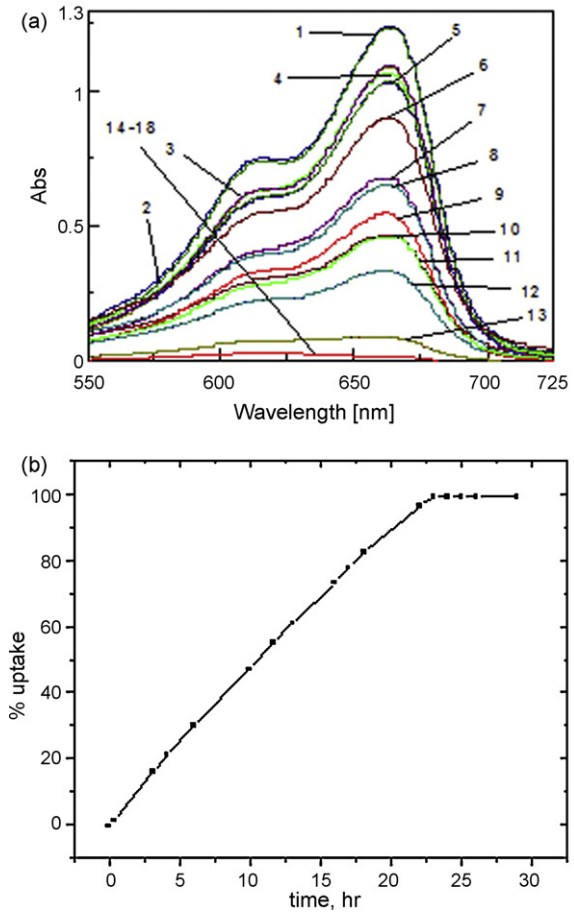

Fig. 9. (a) Time-resolved absorption spectra of adsorption of MB onto cobalt oxide nanoparticles: (1) 0 min, (2) 15 min, (3) 3 h, (4) 4 h, (5) 6 h, (6) 10 h, (7) 12 h, (8) 13 h, (9) 15 h, (10) 17 h, (11) 18 h, (12) 20 h, (13) 22 h, (14–18) 23–29 h; (b) % removal of methylene blue dye versus time on cobalt oxide nanoparticles.

3.3. Adsorption properties of cobalt oxide nanoparticles

Methylene blue (MB) is a cationic dye and has wide applications include coloring paper, silk, etc. [35]. Although methylene blue is not strongly hazardous, it can cause some harmful effects such as vomiting, shock, others [36]. Because dyes are designed to resist breakdown with time, water, exposure to sunlight, soap, and oxidizing agent, conventional wastewater treatment processes cannot be used to remove them [37]. Adsorption techniques have been used to removes dyes but low capacity of some adsorbents is still the main problem. In such, a preliminary study on using the synthesized spinel cobalt oxide as an efficient adsorbent for the methylene blue dye has been carried out in this study. A stock solution of 1000 mg/L of MB dye was prepared by dissolving an appropriate amount of MB dye which was then diluted to the required concentration. Batch adsorption experiments were carried out to investigate the effect of time of contact on the adsorption of MB dye on cobalt oxide. The experiments were carried out in 150 mL conical flask by mixing a pre-weighed amount of cobalt oxide with 25 mL of dye solution and subsequently the solution was stirred at constant temperature and at 200 rpm speed for a specific time then the mixture was centrifuged. The dye concentration in supernatant solution was determined at the characteristic maximum wavelength (665 nm) of the MB dye using UV–vis spectrophotometer.

Adsorption spectra of the dye solutions stirred for different times were recorded and presented in Fig. 9a. It is clear that adsorption of MB dye increases on increasing of time until it reached its maximum at 24 h contact time at which the concentration of the unadsorbed due in the supernatant solution is almost zero. This result is a promising one for the efficiency of cobalt oxide as an efficient adsorbent. Moreover, the removal percentage of dye as contact time increase, which was calculated using the following equation, is presented in Fig. 9b.

$$\%\,\text{removal} = \frac{C_0 - C}{C_0} \times 100$$

where C_0 is the initial concentration of dye (mg/L), and C is the concentration of dye at specific contact time in supernatant solution (mg/L). Fig. 9b shows that the % removal of the MB dye increases gradually from 1.6% to 99.19% as contact time increases from 15 min to 24 h, then this percent remains constant on increasing the contact time. Hence, it can be deduced that the equilibration time for this adsorption process at the current conditions is 24 h. It is worthy to report that adsorption of MB on the three synthesized cobalt oxide products has been studied and it gave the same results. This means that the difference in particle size is not big enough to give change in adsorption properties of the different cobalt oxide products.

4. Conclusions

A very simple, fast, and scalable pathway toward cobalt carbonate microspheres with an average size of 3 μm has been explored using hydrothermal synthesis. Cobalt carbonate microspheres in high yield (94%) were obtained after the hydrothermal treatment of the reported mixture at 120 °C for 0.5 h, and with molar ratio of (1:3) (Co^{2+}:CO_3^{2-}). Different morphologies such as: hexagonal, square, and sheet shaped nanoparticles of Co_3O_4, with an average size of 25 nm were successfully prepared by thermal decomposition of the $CoCO_3$ samples at calcinations 500 °C for 3 h. The optical properties of the as-prepared cobalt oxide nanoparticles revealed the semiconducting behavior by presence of two band gaps whose values (1.45 and 1.85 eV), (1.46 and 1.93 eV), and (1.47 and 1.83 eV) for D, E and F samples, respectively. We believe that this general approach can be extended to prepare some other metal carbonates and their metal oxides. The synthesized Co_3O_4 can be used in some analytical applications such as removal of methylene blue dye, since the % uptake was found to be >99% within 24 h.

Appendix A. Supplementary data

Supplementary data associated with this article can be found, in the online version, at http://dx.doi.org/10.1016/j.materresbull.2012.04.070.

References

[1] H.X. Li, Z.F. Bian, J. Zhu, D.Q. Zhang, G.S. Li, Y.N. Huo, H. Li, Y.F. Lu, J. Am. Chem. Soc. 129 (2007) 8406.
[2] B.H. Wu, C.Y. Guo, N.F. Zheng, Z.X. Xie, G.D. Stucky, J. Am. Chem. Soc. 130 (2008) 17563.
[3] I. Luisetto, F. Pepe, E. Bemporad, J. Nanopart. Res. 10 (2008) 59.
[4] H. Li, R. Liu, R.X. Zhao, Y.F. Zheng, W.X. Chen, Z.D. Xu, Cryst. Growth Des. 6 (2006) 2795.
[5] J. Bachmann, J. Jing, M. Knez, S. Barth, H. Shen, S. Mathur, U. Gosele, K. Nielsch, J. Am. Chem. Soc. 129 (2007) 9554.
[6] L. Zhang, E. Ruh, D. Grutzmacher, L.X. Dong, D.J. Bell, B.J. Nelson, C. Schonenberger, Nano Lett. 6 (2006) 1311.
[7] P. Poizot, S. Gurgeon, L. Dupont, J.M. Tarascon, Nature 407 (2000) 496.
[8] W.Y. Li, L.N. Xu, J. Chen, Adv. Funct. Mater. 15 (2005) 851.
[9] C. Nethravathi, S. Sen, N. Ravishankar, M. Rajamathi, C. Pietzonka, B. Harbrecht, J. Phys. Chem. B 109 (2005) 11468.
[10] D.S. Wang, T. Xie, Q. Peng, S.Y. Zhang, J. Chen, Y.D. Li, Chem. Eur. J. 14 (2008) 2507.
[11] Y. Ding, L. Xu, C. Chen, X. Shen, S.L. Suib, J. Phys. Chem. C 112 (2008) 8177.

[12] J. Ahmed, T. Ahmad, K.V. Ramanujachary, S.E. Lofland, A.K. Ganguli, J. Colloid Interface Sci. 321 (2008) 434.
[13] L. Man, B. Niu, H. Xu, B. Cao, J. Wang, Mater. Res. Bull. 46 (2011) 1097.
[14] X.H. Liu, G.Z. Qiu, X.G. Li, Nanotechnology 16 (2005) 3035.
[15] S.Y. Lian, E.B. Wang, L. Gao, L. Xu, Mater. Lett. 61 (2006) 3893.
[16] Z.G. Wang, X.Y. Chen, M. Zhang, Y.T. Qian, Solid State Sci. 7 (2005) 13.
[17] H.P. Cong, S.H. Hu, Cryst. Growth Des. 9 (2009) 210.
[18] E. Hosono, S. Fujihara, I. Honma, H.S. Zhou, J. Mater. Chem. 15 (2005) 1938.
[19] Y.S. Ding, L.P. Xu, C.H. Chen, X.F. Shen, S.L. Suib, J. Phys. Chem. C 112 (2008) 8177.
[20] X.W. Lou, D. Deng, J.Y. Lee, L.A. Archer, J. Mater. Chem. 18 (2008) 4397.
[21] C.C. Li, X.M. Yin, T.H. Wang, H.C. Zeng, Chem. Mater. 21 (2009) 4984.
[22] M.Y. Nassar, I.S. Ahmed, Polyhedron 30 (2011) 2431.
[23] A.R. Khataee, M.B. Kasiri, J. Mol. Catal. A 328 (2010) 8.
[24] Z. Zhang, J. Kong, J. Hazard. Mater. 193 (2011) 325.
[25] A.N. Chowdhury, A. Rahim, Y.J. Ferdsoi, M.S. Azam, M.M. Hossain, Appl. Surf. Sci. 256 (2010) 3718.
[26] R. Jenkins, R.L. Snyder, Chemical Analysis Introduction to X-ray Powder Diffractometry, John Wiley and Sons, Inc., New York, 1996.
[27] A. Askarinejad, A. Morsali, Chem. Eng. J. 150 (2009) 569.
[28] K. Nakamoto, Infrared and Raman Spectra of Inorganic and Coordination Compounds; Pt. B: Applications in Coordination, Organometallic and Bioinorganic Chemistry, 5th ed., Wiley-Interscience, USA, 1997.
[29] R. Xu, H.C. Zeng, J. Mater. Chem. 8 (1998) 2499.
[30] K.T. Ehlsissen, A. Delahaya-Vidal, P. Genin, M. Figlarz, P.J. Willmann, Mater. Chem. 3 (1993) 883.
[31] M. Salavati-Niasari, F. Davar, M. Mazaheri, M. Shaterian, J. Magn. Magn. Mater. 320 (2008) 575.
[32] M. Herrero, P. Benito, F.M. Labajos, V. Rives, Catal. Today 128 (2007) 129.
[33] M.P. Dare-Edwards, A.H. Goodenough, A. Hammett, P.R. Trevellick, J. Chem. Soc., Faraday Trans. 9 (1983) 2027.
[34] D. Barreca, C. Massignan, S. Daolio, M. Fabrizio, C. Piccirillo, L. Armelao, E. Tondello, Chem. Mater. 13 (2001) 588.
[35] F. Karipcin, E. Kabalcilar, S. Ilican, Y. Caglar, M. Caglar, Spectrochim. Acta A 73 (2009) 174.
[36] J.Z. Yi, L.M. Zhang, Bioresour. Technol. 99 (2008) 2182.
[37] E. Bulut, M. Ozacar, I.A. Sengil, Micropor. Mesopor. Mater. 115 (2008) 234.